T. O. Rocheleau, T. L. Naing, Z. Ren, and C. T.-C. Nguyen, "Acoustic whispering gallery mode resonator with $Q$ >109,000 at 515 MHz," *Tech. Digest*, 2012 IEEE Micro Electro Mechanical Systems Conference, Paris, France, Jan. 29 – Feb. 2, 2012, pp. 672-675.

# ACOUSTIC WHISPERING GALLERY MODE RESONATOR WITH $Q$ > 109,000 AT 515MHZ

*Tristan O. Rocheleau, Thura Lin Naing, Zeying Ren, and Clark T.-C. Nguyen*
*University of California, Berkeley, USA*

## ABSTRACT

A capacitive-gap transduced micromechanical resonator design based on an acoustic whispering gallery mode (WGM) constructed in micro-crystalline diamond has achieved a $Q$ >109,000 at 515MHz, posting an $f{\cdot}Q$ product of >$5.6\times10^{13}$. The key to this performance is anchor-loss nulling by the WGM, as evidenced by comparison of $Q$ values between radial-contour modes and WGM ones on the same disk device, where a 2-3× enhancement of $Q$ is observed. $Q$'s exceeding 100,000 should enable unprecedented RF front-end frequency selectivity and low phase noise oscillators for future communications.

## INTRODUCTION

On-chip, resonators with CAD-definable resonance frequencies and $Q$'s over 30,000 in the upper UHF range (i.e., GHz), if achievable, have the potential to revolutionize compact wireless transceiver design by enabling on-chip RF channel-select filters, as well as integrated oscillators with extremely low phase noise. While efforts over the past few years have yielded great advances, e.g., $Q$ =14,600 at 1.2GHz in [1], still no device with the CAD-definable frequency needed to create single-chip banks of multiple filters has exhibited $Q$'s >30,000 at GHz.

The ongoing quest for higher $f{\cdot}Q$ product demands reductions in both anchor loss and fundamental material loss. Among available materials, theoretical calculations [2] identify diamond as an exceptional material, due to its very high acoustic velocity (~12,000m/s) and its low predicted fundamental phonon scattering rate. To address anchor loss, recent work [3] investigating the use of diamond material for radial-contour mode disk resonators, established the efficacy of using a different support stem material (e.g., polysilicon) to engineer an acoustic mismatch that reduces energy transfer to the stem, in turn reducing loss to the substrate. With demonstrated enhancements in $f{\cdot}Q$ product of up to 6.5× for diamond disks with polysilicon stems versus identical all-polysilicon counterparts, significant $Q$ gains are clearly possible via reduction of anchor loss.

With an intent to further reduce anchor loss, this work explores the use of the same high-$Q$ diamond disks with mismatched polysilicon center stems, but this time designs the electrodes (c.f. Fig. 1) to couple to volume-conserving high-order whispering gallery modes (WGM) that reduce motion at a disk's center, thereby further reducing anchor loss towards unprecedented $Q$'s as high as 109,200 at 515MHz.

## THE WHISPERING GALLERY MODE

The name "whispering gallery mode" was first coined by Lord Rayleigh in the early 1900's while describing acoustic resonances in St. Paul's Cathedral [4]. The original term as applied to building-sized phenomena eventually became the term of choice to describe similar phenomena in micro-optical devices [5], and more recently, in high-order optically excited acoustic microspheres [6]. Low-order acoustic WGM's were in fact first used at the micro-scale in the device of [7], which was dubbed the "wine-glass disk", but was functionally a 2nd order WGM. Higher order WGM's, however, have not yet been explored in an electrically excited micro-acoustic device suitable for RF filter and oscillator applications.

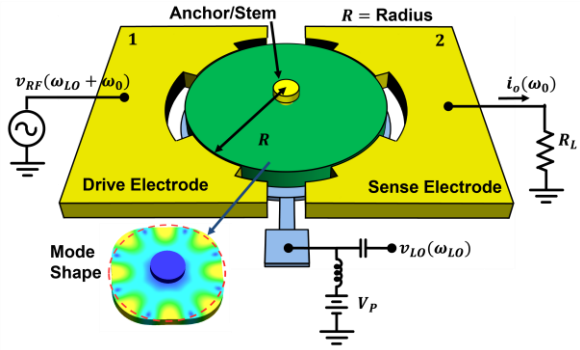


*Fig. 1: Schematic of the whispering gallery mode resonator. Drive and sense electrodes are toothed to interact with only regions of the resonance mode moving with the same phase to maximize coupling.*

In a whispering gallery mode, acoustic waves bounce around the circumference of the disk, but do not penetrate close to the center stem. At resonance, as shown in the inset of Fig. 1 (and later in Fig. 2), a standing wave is produced at the edge of the disk with nearby antinodes moving 180° out of phase, providing a mode-shape that conserves overall volume and thereby induces less motion at the center of the disk than other modes. To illustrate, Fig. 2 presents Coventorware FEM mode-shape simulations confirming that whispering gallery modes with multiple lobe maxima along the circumference of a disk produce much smaller motions at the center of the stem-supported disk (as indicated by the blue color) compared to contour modes, and so should allow higher $Q$.

From [8], the transcendental equations governing the whispering gallery mode frequency, $f_0$, are given by:

$$\left[\psi\left(\frac{\zeta}{\xi}\right)-n-q\right]\left[\psi(\zeta)-n-q\right]=(n\cdot q-n)^2 \qquad (1)$$

$$\psi(x)=\frac{xJ_{n-1}(x)}{J_n(x)}; \qquad q=\frac{\zeta^2}{(2n^2-2)}; \qquad (2)$$

$$\zeta=2\pi f_0 R\sqrt{\frac{\rho(2\sigma+2)}{E}}; \qquad \xi=\sqrt{\frac{2}{1-\sigma}} \qquad (3)$$

where $R$ is disk radius, $\rho$ material density, $\sigma$ Poisson's ratio, $E$ Young's modulus, $n$ mode number, and the $J$'s denote Bessel functions of the first kind. Many such whispering gallery modes with different numbers of lobes

**Table 1: Calculated Parameters for a Diamond Disk WGM Device**

| | | | |
|---|---|---|---|
| **Young's Modulus, E** | 1180 GPa | **Disk Thickness, *h*** | 2μm |
| **Density, $\rho$** | 3500 Kg/m$^3$ | **Bias Voltage, $V_P$** | 15V |
| **Disk Radius** | 17μm | ***Q*** | 30,000 |

| Mode (n) | Frequency (MHz) | $R_x$(kΩ) (100nm gap) | $R_x$(kΩ) (20nm gap) |
|---|---|---|---|
| 2 | 259 | 620 | 1.0 |
| 3 | 397 | 760 | 1.2 |
| 4 | 516 | 820 | 1.3 |
| 5 | 627 | 830 | 1.3 |
| 6 | 735 | 830 | 1.3 |
| 7 | 840 | 830 | 1.3 |
| 8 | 945 | 830 | 1.3 |
| 9 | 1048 | 830 | 1.3 |
| 10 | 1151 | 830 | 1.3 |

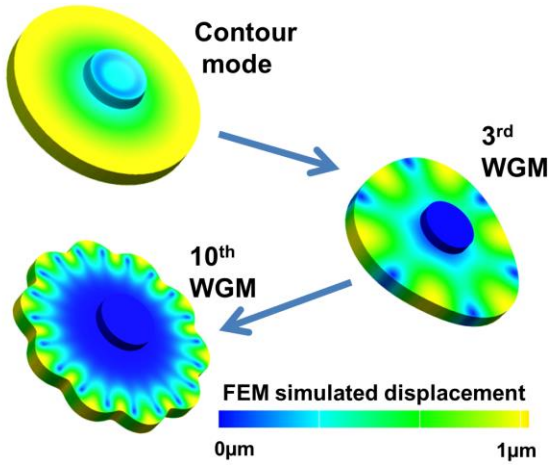


*Fig. 2: FEM analysis of motional amplitude comparing the fundamental contour mode with the 3rd and 10th WGM's. As WGM number is increased, motion at the stem-supported center of the disk can be seen to decrease, reducing anchor loss.*

are possible; the first 10 solutions for a 17μm-radius diamond disk are shown in Table 1.

While the exact frequency solution is dictated by the transcendental equations (1)-(3), Table 1 shows that the resonance frequencies follow a roughly linear dependence on mode number, i.e., much as if they were higher harmonics of a fundamental mode. In essence, a WGM resonator is not so different from a surface acoustic wave (SAW) resonator with the outer diameter of the disk serving as the surface. Here, the frequency of the device can be thought of as determined primarily by the wavelength of the standing acoustic lobes, and thus, by the disk circumference, in turn governed by its radius.

## DEVICE DESIGN AND OPERATION

Pursuant to isolating a specific WGM, the devices of this work employ segmented electrodes, such as shown in Fig. 1, to better align and couple to the lobes of the specific mode desired. Previously demonstrated disk resonators that employed full electrodes spanning the entire disk cannot effectively transduce the WGM, as adjacent lobes of the mode move 180° out of phase with one another, thus nulling the total drive force and output current of the electrode. By selectively removing regions of the electrode, only WGM lobes in phase are coupled. With segmented electrodes, this device can then be excited and sensed as usual, by applying a combined bias plus ac voltage across the input electrode-to-resonator gap to drive the device into WGM vibration; then sensing the ensuing output current at the output electrode. This electrode design has the added advantage of coupling to only the designed WGM, thus suppressing other modes—an important consideration for filter or oscillator design.

For fabrication simplicity, the electrode design of Fig. 1 couples only to WGM lobes in one phase, and not to lobes moving in the opposite phase. Indeed, coupling to the latter would require additional electrode segments that must be excited and detected in the opposite phase. This is certainly realizable, but requires a more challenging fabrication process, so is not done in this initial work. With only half the maximum possible combined electrode-to-resonator overlap area, the electrodes of this work generate only half the available drive force and sense only half the output current, so exhibit 4× larger motional resistance than if it had more complete electrodes.

Alongside frequency, Table 1 also provides predicted values of motional impedance, given by [10]:

$$R_x = \frac{\sqrt{k_r m_r}}{Q\eta^2}; \qquad \eta = V_P \frac{\partial C}{\partial r} \tag{4}$$

where $k_r$ is effective resonator stiffness, $m_r$ is effective resonator mass, $V_P$ is applied bias voltage, and $\partial C/\partial r$ is the overall change in electrode-disk capacitance per unit of radial motion of the resonator integrated over the mode-shape across the electrode. From Table 1, the motional resistance predicted by (4) is nearly independent of mode number for a given disk with constant radius.

If the radius of the disk is allowed to change, however, the motional resistance at a given frequency can be tailored to any desired value, so long as the disk size is not constrained. Specifically, since the $\partial C/\partial r$ term in (1) is directly proportional to the number of motional lobes overlapped by electrodes, while $\sqrt{k_r m_r}$ increases only linearly with increasing lobe number, an increase in the number of lobes reduces the overall motional resistance. So for a given frequency, an increase in disk circumference (as realized by a corresponding increase in radius) serves to reduce motional resistance in a manner comparable to that achieved by arraying of resonators [11], but in this case in a single device. Fig. 3 plots motional impedance versus disk radius and mode number for a 500MHz design with 20nm electrode-to-resonator gaps [12][13], showing resistance reductions with increasing mode number or radius.

The design of a WGM resonator, then, reduces to first determining the wavelength of the surface wave at the

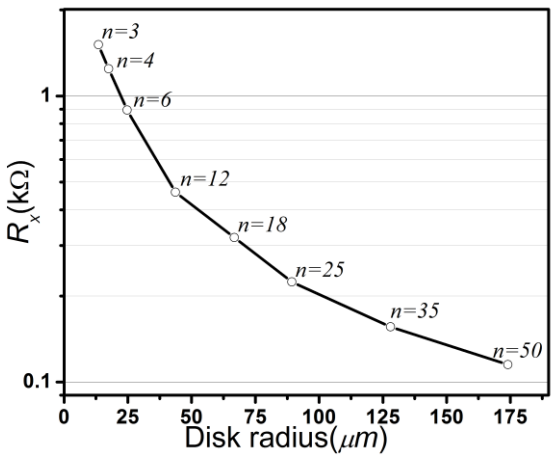


*Fig. 3: Calculated motional impedance for diamond WGM resonators with 20nm capacitive gaps designed for a constant 500MHz frequency as radius and mode number are increased. Here, $V_P$=15V and Q=30,000.*

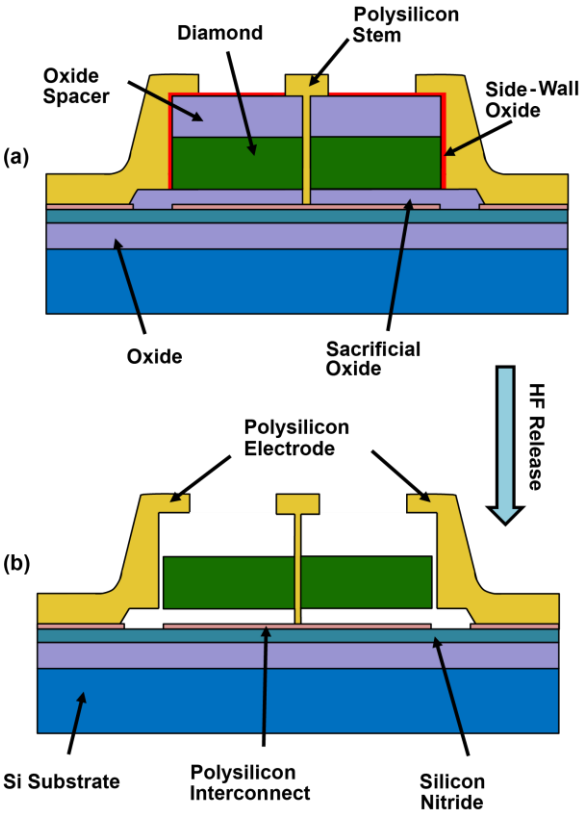


*Fig. 4: Cross-sections of the stem-supported disk (a) immediately before release, with bottom and sidewall high temperature oxide (HTO) sacrificial layers intact; and (b) following release in 49%HF solution to leave the freestanding device.*

desired frequency; then, scaling the disk radius to achieve a circumference equal to an integer multiple of this wavelength that attains the desired value of motional resistance.

## DEVICE FABRICATION

The fabrication process used for the devices presented here closely follows that of [3] and is summarized in the cross sections of Fig. 4. The 2µm-thick microcrystalline diamond film is formed on the sacrificial oxide by first seeding the wafer with diamond nanoparticles to provide nucleation sites, then depositing diamond material via a hot-filament chemical-vapor deposition tool, made by sp3, at 730°C in a 25torr atmosphere with flows of 30sccm $CH_4$, 3000sccm $H_2$, and for doping, a mixture of 2% trimethylboron in $H_2$ flowing at 1sccm.

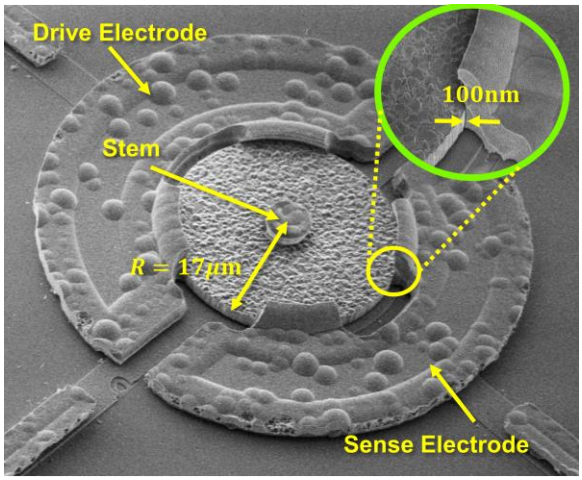


*Fig. 5: SEM showing the fabricated device. The micromechanical resonator consists of a 17µm-radius, 2µm-thick micro-crystalline HF CVD diamond disk. The inset zooms in on the tiny 100nm capacitive gap between disk and electrode.*

## EXPERIMENTAL RESULTS

Using the fabrication process of the preceding section, 17µm diameter diamond disk devices with 100nm capacitive gaps were constructed using electrodes designed to couple to the fourth mode. Fig. 5 presents the SEM of one such device. Despite its segmented geometry, the electrode of Fig. 1 is capable of exciting not only the 4th WGM, but also the radial contour mode. This then allows direct comparison of $Q$'s for these modes.

Devices were tested using a Lakeshore model FWPX probe station to provide a 10µTorr environment while allowing electrical access to devices via probes. To overcome smaller-than-expected output currents caused by the lack of ideal electrodes described earlier, and to maximize the accuracy of extracted $Q$-values, measurements employed the mixing technique of [14] to separate desired motional currents from competing parasitics.

Fig. 6 presents the measured responses in vacuum for a 17µm-radius disk operating in (a) its radial-contour mode at 309MHz with a $Q$~17,300; and (b) in the 4th WGM, at a higher frequency of 511MHz with a higher $Q$~47,900—an overall $f \cdot Q$ increase of 4.6×. This data, measured on the same device, confirms the expectation that anchor losses indeed dominate among loss mechanisms at high frequency, allowing the WGM device with its smaller stem motion to attain significantly higher $Q$.

From the measured curves, the motional resistances of the devices were extracted using the methods of [14] and were found to be 770kΩ and 560kΩ for the contour and whispering gallery modes, respectively. These agree, within the uncertainty of the measurement, with theoretical calculations using (4) on this electrode shape together with measured $Q$ values and a 100nm electrode-to-resonator gap spacing.

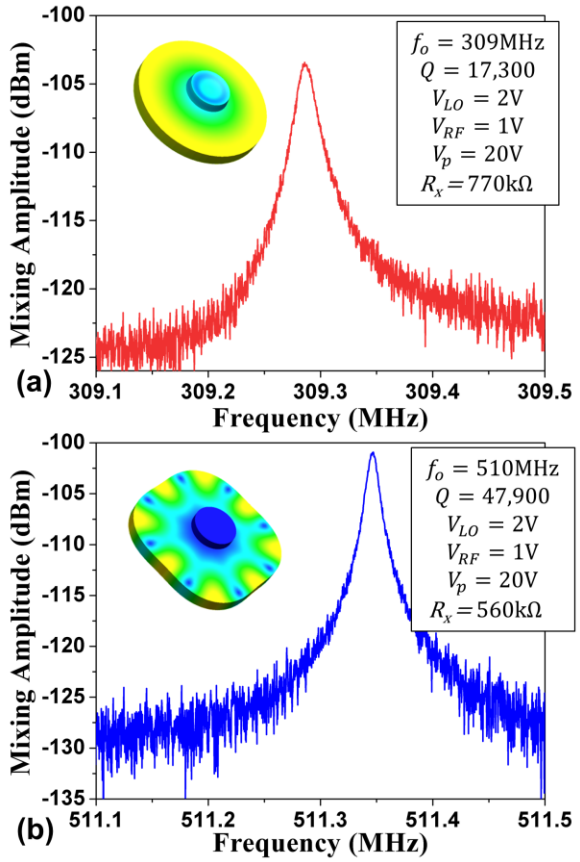


*Fig. 6: Measured responses for diamond disk resonators operating (a) in the radial contour mode with Q=17.3k at 309MHz; and (b) in the 4th whispering gallery mode for the same device with Q=47.9k at 510MHz, which constitutes a 4.5times improvement in f·Q product.*

One remaining question is whether or not the stem isolation provided by the WGM device is enough to eliminate anchor losses to the point of revealing the maximum $Q$ value permitted by structural material losses. To shed some light on this, Fig. 7 presents the measured frequency characteristic for another of the same WGM disk devices, this one exhibiting the best performance among ~60 measured devices, with a startlingly high $Q$ =109,000 at 515MHz. This is the highest $Q$ measured to date at ~500MHz for any on-chip room temperature resonator, yielding an $f{\cdot}Q$ product of $5.6{\times}10^{13}$, which is the highest so far demonstrated in diamond structural material. Does this represent the limit of the hot filament CVD diamond material used here? It's anyone's guess, but theory does predict that even higher $Q$'s should be possible.

## CONCLUSIONS

By designing electrodes to couple to a specific WGM in an HF CVD diamond disk, the WGM has been shown to greatly enhance $f{\cdot}Q$ product by suppressing anchor losses, in particular posting a record-setting $Q$ of 109,200 at 515MHz, the highest $Q$ reported to date in this frequency range for a room-temperature acoustic device. The corresponding $f{\cdot}Q$ of $5.6{\times}10^{13}$ is comparable to previous best reported values for FBAR resonators [15], but with the marked advantage of having a CAD-definable frequency dependent mainly on lateral dimensions. The improved anchor isolation and very high $Q$'s at UHF should enable unprecedented RF front-end frequency selectivity and low phase noise in oscillators for future portable communications. Additionally, the reduced motion at the center of the WGM disk suggests the possibility of larger anchors or the use of simpler non-self-aligned processes, greatly reducing cost and difficulty of fabricating such devices in a production setting.

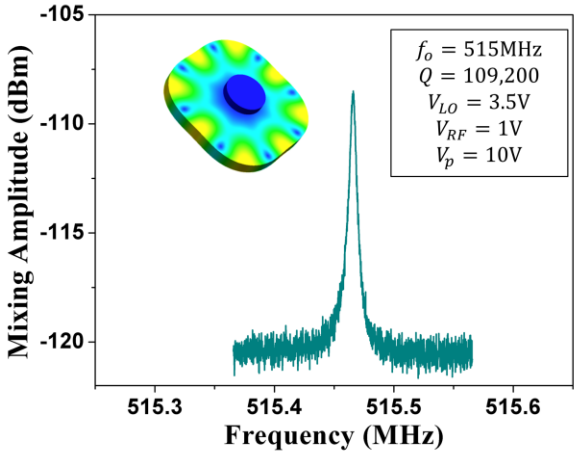


*Fig. 7: Measured frequency characteristic for a second diamond disk device with a remarkable Q=109.2k at 515MHz. While of the same diamond resonator design, this device did not have fully notched electrodes, so had significantly less coupling.*

***Acknowledgement***: This work was supported by the DARPA ART program.

## REFERENCES

[1] S. Li, Y. Lin, Y. Xie, Z. Ren, and C. T.-C. Nguyen, *Proceedings*, IEEE Int. Conf. on MEMS, 2004, pp. 821-824.
[2] R. Tabrizian, M. Rais-Zadeh, and F. Ayazi, *Proceedings*, Transducers, June 2009, pp. 2131-213.
[3] M. Akgul, et al., *Proceedings*, IFCS-EFTF, May 2011, pp. 1036-1039.
[4] Lord Rayleigh, *Philos. Mag.* 20, pp. 1001, 1910.
[5] C. G. B. Garrett, W. Kaiser, and W. L. Bond, *Phys. Rev.*, vol. 124, pp. 1807–1809, 1961.
[6] M. Tomes, and T. Carmon, *Phys. Rev. Lett.* 102, p. 113601, 2009.
[7] M. A. Abdelmoneum, M. U. Demirci, and C. T.-C. Nguyen, *Proceedings*, IEEE Int. Conf. on MEMS, Jan., 2003, pp. 698-701.
[8] M. Onoe, *J. Acoust. Soc. Amer.*, vol. 28, no. 6, pp. 1158–1162, 1956.
[9] J. Wang, et. al, *Proceedings*, IEEE Int. Conf. on MEMS, Jan., 2004, pp. 641-644.
[10] Y.-W. Lin et al., *IEEE Journal of Solid-State Circuits*, Vol. 39, No. 12, pp. 2477-2491, 2004.
[11] M.U. Demirci, and C.T.-C. Ngueyn, *Journal of Microelectromechanical Systems*, Vol. 15, No. 5, pp. 1419-1436, 2006.
[12] M. Akgul, B. Kim, Z. Ren, and C.T.-C. Nguyen, *Proceedings*, Hilton-Head Conf., Jun. 2010, pp. 467-470.
[13] Tiffany J. Cheng , Sunil Bhave, *Proceedings*, IEEE Int. Conf. on MEMS, 2010, pp. 695-698.
[14] A. Wong and C.T.-C. Nguyen, *Journal of Microelectromechanical Systems*, Vol 13, No. 1, pp. 100-112, 2004.
[15] E. Hwang and S. A. Bhave, *Proceedings*, IEEE Transactions on Electron Devices 58(8), 2011, pp. 2770-2776.